



Numerical Prediction of the Impact Fracture of a Projectile Through Oblique Target

Ju Suk Yang^{1,2} · Min Kuk Choi¹ · Chun-Gon Kim²

Received: 6 February 2023 / Revised: 10 April 2023 / Accepted: 10 May 2023 / Published online: 29 June 2023
© The Author(s), under exclusive licence to The Korean Society for Aeronautical & Space Sciences 2023

Abstract

In modern warfare, oblique penetration is frequently observed when a penetration warhead mounted on a guided missile hits the target. When oblique penetration occurs on hard targets, such as reinforced concrete, the projectile experiences complex stress states along with tensile and compression stresses that can result in the deformation and fracture of the projectile. Therefore, the survivability of the projectile should be determined at the design phase. Structural survivability was assessed here through a correlated simulation considering a case where the projectile was fractured while penetrating into a 30° inclined concrete target at 333 m/s. For correlated simulation, we obtained the dynamic constitutive equation and fracture properties of the projectile material (AISI4340 steel) up to a strain rate of 1500 s⁻¹. Furthermore, concrete material coefficients related to the strain rate sensitivity were calibrated using the test database. Computational analysis result agreed well with the actual test result.

Keywords Projectile · Fracture · Oblique penetration · Concrete target

1 Introduction

High-value key military installations, such as enemy's main command posts, are either fixed ground-based targets or hard and deeply buried targets (HDBTs). This increases the demand for advancing the penetration warheads that can effectively hit these targets. Analyzing penetration phenomena and evaluating the penetration performance of penetration warheads according to their design factors using actual warheads are challenging, because these are expensive and time-consuming, which is an important factor in the process of designing and developing penetration warheads. Several studies have been conducted on the penetration of projectile into concrete structures, and various methods have been proposed for evaluating its penetration performance. Young [1] performed penetration tests with various design factors of penetration warheads on several targets and proposed an

empirical formula that can calculate the penetration depth. Forrestal [2, 3] analyzed vertical penetration of a projectile into a concrete target and proposed an empirical formula for calculating the penetration depth of the vertical penetration based on the cavity expansion theory.

Generally, oblique penetration occurs much more frequently than vertical penetration for the penetrating warheads during the process of operating a weapon system. When a penetration warhead hits a concrete target with high speed at an inclined angle, the projectile and target experience complex loads that are asymmetrically mixed with tension and compressive loads [4]. Thus, the projectile may deform and fracture, which can greatly affect its performance by damaging its internal parts and degrading its penetrability. Through nonlinear computational analysis, Liu et al. [5, 6] confirmed the deformation of a projectile by performing oblique penetration analysis in concrete with a projectile that was treated as a deformable body rather than a rigid body. Therefore, it is important to ensure warhead survivability while designing penetration warheads.

Studies on warhead survivability have been limited and rarely disclosed due to security and other issues. Zukas [7] presents an example of deformation and destruction of a projectile in various penetration processes. In his view, the deformation caused by the bending of a projectile in oblique

Ju Suk Yang and Min Kuk Choi have contributed equally to this work.

✉ Chun-Gon Kim
cgkim@kaist.edu

¹ Agency for Defense Development, Daejeon, South Korea

² Korea Advanced Institute of Science and Technology, Daejeon, South Korea

penetration was considered as an analytically intractable problem. Air Force Research Laboratory (AFRL) in the United States manufactured projectile high-strength alloys to ensure warhead survivability. They conducted various basic studies to investigate the fracture mechanics of projectile and implement them to simulate the destruction of projectile through computational analysis [8]. Yoo et al. [9] performed a computational analysis using the cavity expansion theory on the target resistance to evaluate penetration performance with respect to various design factors, and performed a projectile deformation simulation in oblique penetration. Therefore, to assess the warhead survivability for simulating the deformation of the projectile, structural survivability assessment must be carried out through correlated simulation.

To assess the structural survivability of the penetration warhead through correlated simulation with concrete target penetration, it is necessary to model the physical properties that can simulate the behavior of the projectile and the target under extreme load conditions, such as high pressure and high strain rate. In general, material of the projectile is high-strength steel. According to Lim [10], penetration warheads undergo body deformation and destruction at various strain rate ranging from 0.001 to $10,000 \text{ s}^{-1}$. As plastic deformation progresses, high-strength steels show strain hardening behavior according to the strain rate. To simulate such behavior, various studies have been conducted to describe the stress and strain relationship of the material in the dynamic region. Johnson and Cook [11] proposed the dynamic constitutive equation of the material through the Hopkinson bar test. Huh et al. [12] confirmed the dynamic behavior according to the crystal structure of the material and evaluated and proposed the dynamic constitutive equation. Shin et al. [13] investigated the characteristics of the dynamic constitutive equations published before and presented a guideline for the selection of constitutive equations.

To assess the structural survivability, a constitutive equation for the material of the projectile is necessary. Furthermore, a fracture model is required to simulate the destruction of the projectile during penetration. Fracture models can be divided as physics-based fracture models (continuum damage mechanics model) [14]; micromechanics models [15, 16] based on the evolution of void; and phenomenological fracture models that simulate strain and damage at the onset of fracture. Phenomenological models have been studied by many researchers and applied to commercial computational analysis programs [17]. Wierzbicki et al. [18] investigated the fracture models proposed by various researchers and confirmed their ability to predict fracture. Bai and Wierzbicki [19] proposed a fracture model by introducing stress triaxiality and Lode angle, expressed as a third-order invariant of stress tensor, as a variable in a fracture model, and deriving the equivalent strain-based fracture model using the existing Mohr–Coulomb model. Lou et al. [20] proposed a fracture

model that phenomenologically simulates void nucleation, void growth, and void coalescence with stress triaxiality and Lode angle parameters as variables. However, the proposed model cannot describe the effect of the strain rate of the material, and only a few studies have investigated the fracture model of the material in the dynamic domain. Roth and Mohr [21] measured the fracture strain with tensile velocity and modified the Hosford–Coulomb fracture model using the strain rate function of the Johnson–Cook model. Lim [10] measured the fracture strain at various strain rates of the DP980 steel sheet and analyzed the fracture mechanism according to the strain rate. He modified the Lou model [20] by adding terms representing strain-rate dependency.

Studies on the fracture properties related to impact problems primarily applied the Taylor impact test. Teng et al. [22] performed the Taylor impact test and confirmed that three modes of fracture appeared, and applied ductile failure criteria to numerical analysis and verified them. Zhang et al. [23] evaluated five fracture models in the Taylor impact test, and Xiao et al. [24] proposed a Lode-dependent fracture model to predict the shear cracking in the Taylor impact test of Al2024. As such, various ductile fracture models for metals have been proposed and applied to impact problems. However, only a few models have been used directly in the assessment of the survivability of penetration warheads. In the present study, the usefulness of these models will be examined.

Concrete is widely used as a structural material for buildings and protective materials due to its high compressive strength, durability, and various environmental resistance. For the analysis of penetration in concrete, property modeling that can express the behavior of concrete is required. In the extreme environment of the penetration process, concrete materials show complex and nonlinear behavior due to its inhomogeneity and characteristics. To model strain–stress relations, pressure hardening, strain rate dependency, damage, and fracture under extreme load conditions, many researchers have proposed mechanical property models for concrete, such as RHT model [25], K&C model [26], and CSC model [27]. Among them, the RHT model is pre-loaded in commercial finite-element analysis software, such as LS-DYNA, and is widely used in high-speed impact analysis and penetration analysis. Hansson and Skoglund [28] performed the penetration analysis of projectile with respect to the variables of the RHT model and found that the coefficients for damage accumulation and residual strength surface are sensitive to the results of analysis. The team corrected the appropriate coefficients for predicting the test results. In addition, Shin et al. [29] showed that the conservative effect of strain rate and the simple linear crack softening model in the existing RHT model have limitations in simulating the dynamic behaviors shown in experimental results. Therefore, to obtain accurate target properties, a process of calibration

of the coefficients that can simulate the results of the penetration test is necessary.

This study proposes a new numerical technique for predicting impact fracture in a real-scale scenario, where a projectile penetrates an inclined concrete target. We first tested projectile material in the quasi-static, intermediate strain rate and high strain rate regions to obtain stress–strain data with respect to strain rates and then obtained coefficients of a dynamic constitutive equation. To construct a fracture model, the test method by Lim [10] was used to obtain fracture strain under three load path conditions (shear, uniaxial tension, and plane strain) and various strain rate conditions. The MMC model coefficients proposed by Bai and Wierzbicki [19] were calibrated for each strain rate and applied to the LS-DYNA GISSMO model. In addition, to obtain accurate target properties, a vertical penetration test of the penetrating warhead on a concrete target was performed using a 155-mm smoothbore gun. The test result were compared with the numerical analysis results, and the coefficients of the concrete material model that can best simulate the penetration depth were obtained. Using these material properties of projectile and concrete target, the results of the existing penetration test on an oblique concrete target [30] were compared with the results of correlated simulation, and the structural survivability of the warhead was assessed.

2 Properties of Projectile Material

2.1 Constitutive Equation of Projectile Material

Generally, high-strength steel is used to protect the contents of a penetration warhead during the penetration process. The projectile used in the test [30] is AISI4340 steel, which exhibits high strength and toughness. For reliable penetration analysis, material property modeling that can accurately represent the behavior of materials in the dynamic region is critical. Thus, tensile tests with various strain rates were performed and coefficients of the dynamic constitutive equation were obtained.

First, tensile tests were performed with strain rates ranging from 0.001 s^{-1} to several thousands s^{-1} to obtain material properties considering the strain rate. Considering the effect of the projectile manufacturing process, specimens were obtained using waterjet processing of a finished AISI4340 steel projectile. A sheet was used to perform specimen testing. In the quasi-static strain rate, a tensile tester developed by INSTRON was used. In the intermediate strain rates of 0.1, 1, 10, and 100 s^{-1} , a high-speed material testing machine developed by Lim [31] and Huh et al. [12] was used. The high-speed material testing machine is a servo-hydraulic type high-speed tensile testing machine, with a maximum speed of 7.8 m/s and the maximum strain rate that can be applied

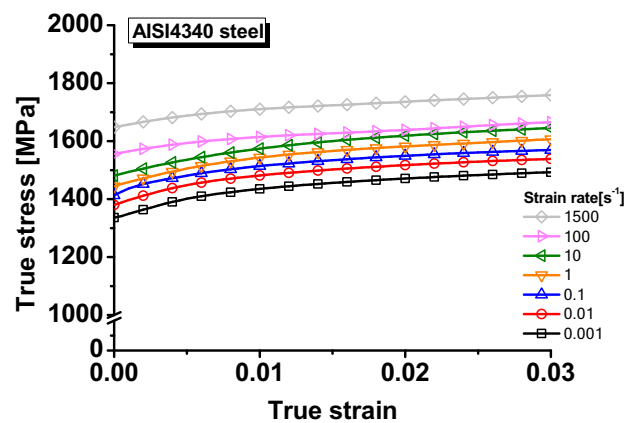


Fig. 1 True stress–true strain curve for AISI4340 steel

to the specimen ranges to several hundreds s^{-1} . The load applied on the specimen was measured using a piezoelectric type load cell, and the specimen strain was measured by capturing the specimen deformation using a high-speed camera and analyzing it with digital image correlation (DIC) after the test. In the high strain rate over 100 s^{-1} , tensile properties were obtained using the tension split Hopkinson pressure bar. The design of the tensile split Hopkinson bar, and the size and shape of the specimens used in the tensile test were adopted from the study of Huh et al. [32]. In the Hopkinson bar test, the stress–strain curve of the material was obtained by analyzing the stress wave in the incident bar and transmission bar.

Through tensile testing, the engineering stress–engineering strain curve was obtained, and the yield stress was determined using the 0.2% offset method. Using the engineering stress–engineering strain curve, the true stress–true strain curve at each strain rate was obtained, which is shown in Fig. 1. In the case of AISI4340 steel, it can be seen that strain hardening and strain rate hardening phenomena appear at the same time. At this time, the uniform strain in the measured data is about 3%, and the size of the strain region is too limited to apply to the numerical analysis. In addition, it is necessary to extend the area of material properties applied to the numerical analysis through interpolation between each strain rate section. Therefore, a material model capable of expressing the dynamic behavior of the material was selected and simulated, and the result was applied to the analysis.

Material property models that can express the dynamic behavior of materials can be divided into two types; ones that use the theory of material deformation, and simple empirical ones. The types of models vary greatly according to the behavior of materials. A study by Huh et al. [12] introduced a dynamic material property model according to the internal lattice structure (BCC, FCC, and HCP) of metal materials, and compared the performance and evaluation results of each material property model. As a result, for a material of BCC

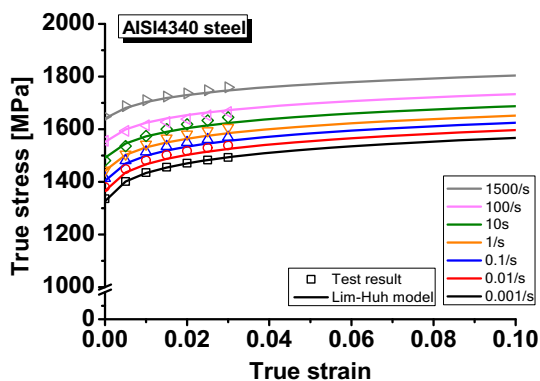


Fig. 2 Fitted result of Lim–Huh model for AISI4340 steel

structure, which is the internal lattice structure of AISI4340 steel, the model proposed as follows has been shown to well express the characteristics of dynamic deformation behavior with respect to strain rate. Therefore, the true stress–true strain curve in Fig. 1 was fitted with the model proposed by Lim [31] and Huh et al. [12] as shown in the equation below

$$\bar{\varepsilon}_f = \left\{ \frac{A}{c_2} \left[c_3 + \frac{\sqrt{3}}{2 - \sqrt{3}} (1 - c_3) \left(\sec\left(\frac{\bar{\theta}\pi}{6}\right) - 1 \right) \right] \left[\sqrt{\frac{1 + c_1^2}{3}} \cos\left(\frac{\bar{\theta}\pi}{6}\right) + c_1 \left(\eta + \frac{1}{3} \sin\left(\frac{\bar{\theta}\pi}{6}\right) \right) \right] \right\}^{-\frac{1}{n}}, \tag{2}$$

$$\sigma(\varepsilon, \dot{\varepsilon}) = A(\varepsilon + \varepsilon_0)^n \times \frac{1 + q(\varepsilon)\dot{\varepsilon}^m}{1 + q(\varepsilon)\dot{\varepsilon}_r^m} \quad \text{where} \quad q(\varepsilon) = \frac{q_1}{(\varepsilon + q_2)^{q_3}}, \tag{1}$$

where ε is the equivalent plastic strain, $\dot{\varepsilon}$ is the strain rate, $\dot{\varepsilon}_r$ is the reference strain rate, and $A, \varepsilon_0, n, q_1, q_2, q_3, m$ are the material constants. The fitting coefficients are shown in Table 1 and the fitting results are shown in Fig. 2. It can be seen that the Lim–Huh model well expresses the projectile material behaviors with respect to various strain rates.

2.2 Fracture Model of Projectile Material

For the analysis of projectile survivability after target penetration, fracture properties are needed, as well as the mechanical properties that can be expressed by the stress–strain relationship of the projectile material. Fracture properties are the properties that show the behavior and characteristics of a material up to the failure of the material. It is necessary to check whether the material fails under specific load

conditions. Most engineering materials can be roughly classified into ductile materials and brittle materials. AISI4340 steel is a ductile material that reaches fracture with plastic deformation. From the microscopic perspective, the nucleation, growth, and coalescence of void lead to the formation of macroscopic cracks and the material failures. Research on fracture from the microscopic perspective has been conducted for a long time. However, due to the complexity of formulas, ambiguity in determining coefficients, and difficulty in applying numerical analysis, phenomenological models have been proposed. Phenomenological models use stress and strain values based on continuum mechanics to establish a weighting function and predict fracture when the integral value of the weighted function for the plastic strain increment at a point in a material reaches a threshold value. Bai and Wierzbicki [19] measured the fracture strain of a Al2024 material according to the stress state that can be expressed as the stress triaxiality η and the Lode angle parameter $\bar{\theta}$, and derived the Mohr–Coulomb model based on strain to construct the following phenomenological model:

where c_1, c_2, c_3 are material constants. c_1 is “friction” coefficients, c_2 is shear resistance, and c_3 is Lode angle-dependent material constant.

As the strain rate increases, the temperature accumulated during the deformation of the material, the increase in dislocation density can trigger the change in fracture mechanism [10, 21, 33]. Thus, the fracture behavior could be dependent on the strain rate. Therefore, in this study, the fracture strain of AISI4340 steel was measured with respect to the strain rate.

Tensile tests were conducted using a high-speed tensile tester and a tension split Hopkinson pressure bar from 0.001 to 1500 s⁻¹, and fracture strain was obtained under pure shear, uniaxial tension, and plane strain conditions for each strain rate. More than three tests per specimen were conducted to confirm the repeatability of the test, and the procedure of the test, the shape of the specimen, and the tensile speed for different strain rate were referred to Lim [10].

During the tensile test, the surface of the specimen was captured with a high-speed camera, and the local fracture strain was measured through image analysis using the digital

Table 1 Calibration result of Lim–Huh model for AISI4340 steel

A	ε_0	n	q_1	q_2	q_3	m
1702	1.8 e ⁻³	0.041	0.209	8.9 e ⁻⁴	0.118	0.047

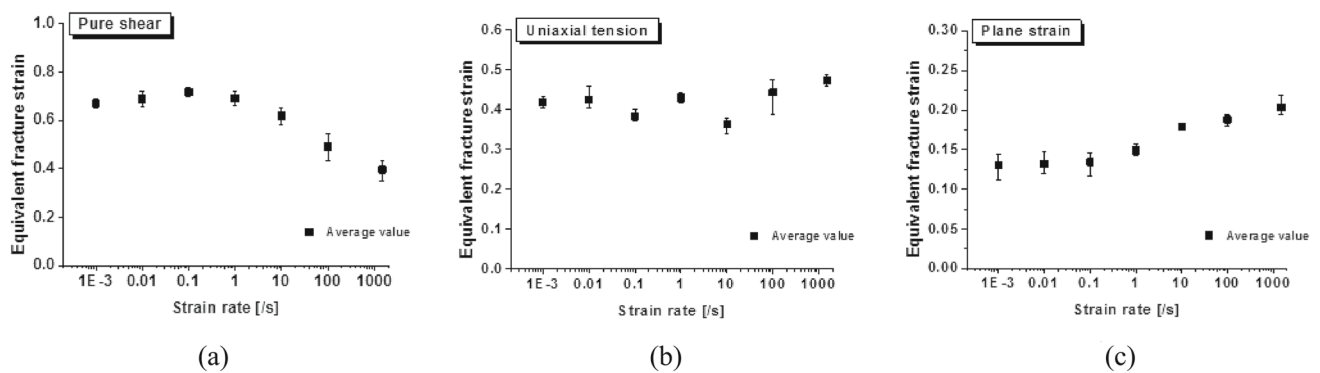


Fig. 3 Fracture strain with various strain rates: **a** pure shear; **b** uniaxial tension; **c** plane strain

Table 2 Calibration results of MMC fracture model with various strain rates

Strain rate	A	n	c_1	c_2	c_3
0.001	1702.44	0.0419	0.0712	881.3	0.9096
0.01	1727.52	0.0400	0.0685	893.82	0.9075
0.1	1755.74	0.0381	0.0662	904.22	0.9014
1	1787.09	0.0359	0.0569	917.43	0.8996
10	1822.39	0.0338	0.0429	919.2	0.8871
100	1861.83	0.0315	0.0308	935.7	0.8897
1500	1914.16	0.0286	0.0194	955.1	0.8872

image correlation technique described above. ARAMIS was used as the DIC software, and strain was measured based on a facet size of $0.1 \times 0.1 \text{ mm}^2$. The in-plane strain can be measured by image analysis, and strain in the thickness direction can be calculated from the planar strain measured based on plastic incompressibility. The equivalent strain to fracture can be calculated by computing and adding the equivalent strain increment using the yield model through the strain increment in each direction. The results of the fracture strain measured with respect to each load condition and strain rate are shown in Fig. 3. As seen in the steel materials in general, the specimen shows decreasing fracture strain as the stress triaxiality increases. In the case of pure shear, as shown in Fig. 3a, the change with respect to the strain rate is not significant in the low-speed region. As the strain rate increases, the fracture strain decreases. Similar to Lim and Huh [34], negative strain rate sensitivity was observed, which can be attributed to the formation of adiabatic shear bands at high strain rates. In the case of uniaxial tension, as shown in Fig. 3b, no significant strain rate sensitivity was observed. However, in the case of plane strain, as shown in Fig. 3c, the fracture strain showed a positive dependency on the strain rate. This seems to be due to the increasing size of the voids resulting from the temperature-induced softening effect caused by the plastic work.

Using the fracture strain data with respect to strain rate under the stress state, the coefficients of the modified Mohr–Coulomb model in Eq. (2) were calibrated at each strain rate.

Since it is difficult to maintain the proportional load due to the local deformation of the specimen during the tensile test, the stress state of the fracture strain data to be used in constructing the fracture model was expressed as a combination of mean values as in Lim [10]. Table 2 shows the coefficients of the modified Mohr–Coulomb model at each strain rate, and Fig. 4 shows the three-dimensional fracture surface for each strain rate. Points represent the experimental data, and the solid lines represent the plane stress condition.

To compare the fracture surface at different strain rates, the two-dimensional fracture loci with respect to strain rate under plane stress conditions were compared and are illustrated in Fig. 5. The trend with respect to strain rate is similar to the result of fracture strain measurements. In the negative triaxiality region, the fracture locus decreased as the strain rate increased. In the triaxiality region after the uniaxial tension, the fracture locus also increased as the strain rate increased.

In general, since the material subjected to load was deformed under a complex loading path rather than a proportional loading path, the fracture prediction at this point can be considered by introducing the following damage function based on the constructed fracture model $\hat{\epsilon}_f(\eta, \bar{\theta})$

$$D = \int_0^{\bar{\epsilon}_f} \frac{d\bar{\epsilon}_p}{\hat{\epsilon}_f(\eta, \bar{\theta})}. \quad (3)$$

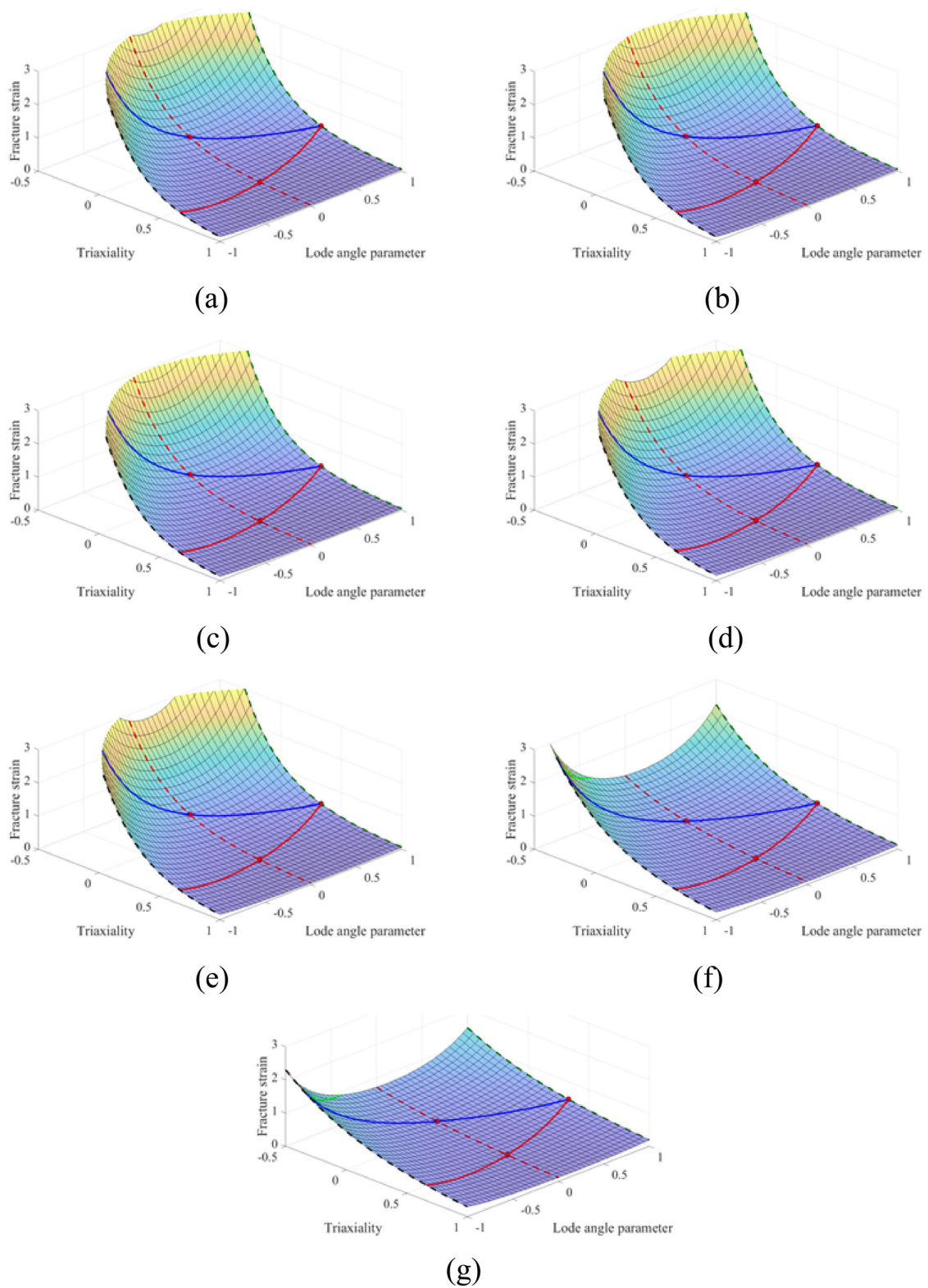


Fig. 4 3D fracture surface with various strain rates: **a** 0.001; **b** 0.01; **c** 0.1; **d** 1; **e** 10; **f** 100; and **g** 1500 s⁻¹

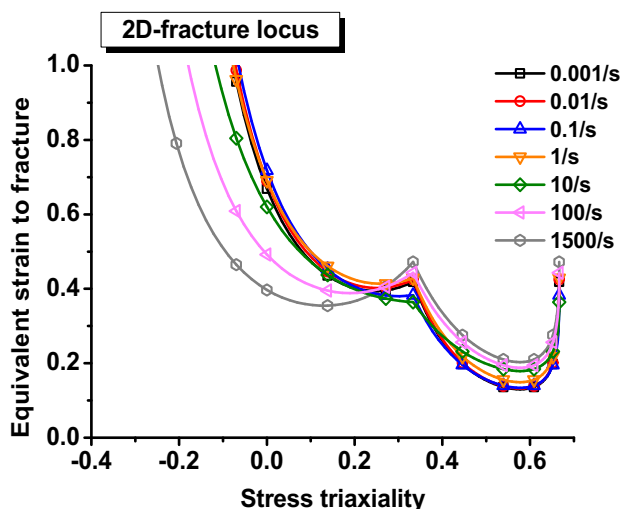


Fig. 5 2D fracture loci with various strain rates

2.3 Application to Computational Analysis

The determined constitutive equation and fracture model for AISI4340 steel were applied to computational analysis using LS-DYNA's material cards. In the case of the constitutive equation, the size of the strain region applied to the analysis was expanded and entered as piecewise linear data with respect to strain rate using *MAT_024.

The fracture model was applied to computational analysis using *MAT_ADD_DAMAGE_GISSMO. The GISSMO, which is Generalized Incremental Stress-State-dependent damage MOdel, is a tool that computationally simulates ductile fracture with the loading path and various fracture factors using the damage value in Eq. (3) and thus is practical for the application to numerical analysis [17]. The fracture surface at each strain rate for AISI4340 steel was tabulated and applied according to the triaxiality and Lode parameter. The Lode angle and Lode parameter in the modified Mohr–Coulomb model were converted according to the study of Lou et al. [35]. When applying the fracture model with respect to strain rate, the LCSRS parameter of GISSMO was used to input the scale factor with respect to strain rate and triaxiality based on the fracture surface in the quasi-static region.

According to Körgesaar [36] and Körgesaar et al. [37], fracture is a locally occurring phenomenon. In computational analysis using a ductile fracture model, fracture is known to be dependent on the density of the element. The GISSMO can use the LCREGD parameter to regularize the mesh size sensitivity in computational analysis. This helps in applying a fracture model based on the fracture strain measured in the local microregion of a specimen to evaluating the fracture of large structures. In this study, the size of a specimen for the fracture strain measurement and that of the projectile for the warhead penetration test are different. Thus, a mesh size-dependent regularization factor is essential. In this study,

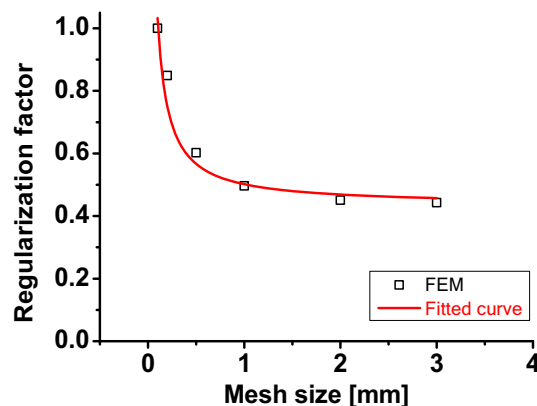


Fig. 6 Mesh size regularization

the results of mesh size-dependent regularization were introduced to show the following regularization equation [38]:

$$r(x) = \frac{1}{\bar{\epsilon}_f} \ln\left(\frac{a}{x} + b\right), \quad (4)$$

where $r(x)$ is regularization factor, x is mesh size, and a and b are fitting coefficients. For regularization, finite-element analysis was performed on a uniaxial tensile specimen with a mesh size of 0.1–3 mm. The reference fracture strain is the fracture strain measured in the 0.1-mm region. As a result of finite-element analysis, the regularization factor with respect to the mesh size and the curve of Eq. (4) fitted with $a = 0.0328$ and $b = 1.1934$ are shown in Fig. 6. As the mesh size increased, the regularization factor converged. Through GISSMO, the fracture surface with respect to strain rate and mesh size regularization were applied to identify the loading path history and degree of damages in the projectile deformation during penetration. When the damage accumulates and reaches a threshold, element was deleted.

3 Target Properties

Analysis on concrete penetration requires precise modeling of the property of concrete. The RHT model is widely used in penetration analysis, but property calibration requires complex and various types of tests. Due to these practical issues, LS-DYNA supports automatic generation of material coefficients corresponding to an unconfined compressive strength of 35–140 MPa through interpolation. However, according to Cho et al. [39], the material coefficients calibrated from the numerical results consistent with experimental data are used for the accuracy of the analysis. Therefore, in this study, a 155 mm smoothbore gun was utilized to conduct a vertical penetration test of a projectile on a concrete target for accurate target property calibration. After comparing the test data with the results of computational analysis, the coefficients of

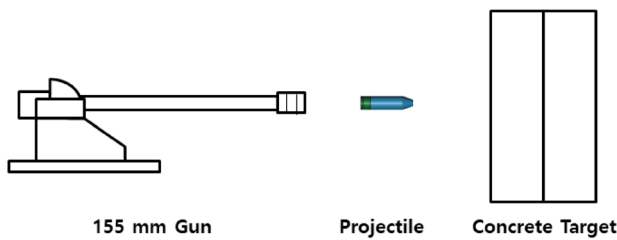


Fig. 7 Schematic diagram of 155 mm gun test

Table 3 Result of 155 mm gun test

Penetrating warhead		Impact speed	Angle of impact	Angle of attack	Penetration depth
Diameter	Weight				
155 mm	47 kg	379 m/s	Perpendicular (90°)	0°	680 mm

the RHT model that best simulate the penetration depth were obtained.

3.1 Smoothbore Gun Test

In the smoothbore gun test, a propelling charge and a test object are loaded into the smoothbore gun and fired to hit the test object on a target. The vertical penetration test of a projectile on a concrete target was conducted using a 155-mm smoothbore gun (Fig. 7). The smoothbore gun test equipment can fire projectiles up to 47 kg, and has a maximum allowable pressure of 55,000 psi and a muzzle energy of up to 20 MJ. The test projectile was made of AISI4340 steel (155-mm diameter and 47-kg weight). The target was set up by stacking two layers of reinforced concrete with an unconfined compressive strength of 5000 psi and dimensions of 3000 × 3000 × 600 mm³. The distance between the smoothbore gun and target was about 19 m. To measure the impact speed and impact posture of the test projectile, high-speed photography was performed using a high-speed camera near the target.

The results of the smoothbore gun test are shown in Fig. 8 and Table 3. The impact velocity was 379 m/s, and the projectile hits the target of two slabs with the angle of attack at 0°. The test projectile penetrated the first slab and then stopped at the second, with a penetration depth of 680 mm. After the test, the test projectile was recovered and examined. No significant deformation or fracture was observed in the test projectile.

3.2 Computational Analysis of Smoothbore Gun Test

Computational analysis was carried out to calibrate the material coefficient in the RHT model using the test results. The RHT model considers the effects of pressure hardening, strain



Fig. 8 Result of 155 mm gun test

hardening, strain rate hardening, damage-induced softening, and shear strength reduction. The material coefficients include coefficients defining the EOS, coefficients related to the limit surface, strain rate-related coefficients, and damage coefficients. Among these, strain rate-related coefficients have been introduced as the concept of Dynamic Increase Factor (DIF) derived from many experimental observations, whose default value is expressed as a linear function on the logarithmic scale of strain rate. To improve the simulation accuracy of DIF related experiments, the European CEB formula [40] and Malvar and Ross [41] have proposed a bilinear form in which the slope sharply increases at a certain strain rate. Shin et al. [29] indicated that the default value of the strain rate-related coefficient in the RHT model may be underestimated in the range after a certain strain rate. Therefore, in this study, strain rate-related coefficients were calibrated to obtain the penetration depth close to the experimental value.

In LS-DYNA, the strain rate-related coefficients in the RHT model are represented by BETAC (β_c) and BETAT (β_t) [42], and the DIF equation is expressed by Eq. (5)

$$F_r^{c/t}(\dot{\epsilon}_p) = \begin{cases} \left(\frac{\dot{\epsilon}_p}{\dot{\epsilon}_0^{c/t}}\right)^{\beta_{c/t}} & \dot{\epsilon}_p \leq \dot{\epsilon}_p^{c/t} \\ \gamma_{c/t} \sqrt[3]{\dot{\epsilon}_p} & \dot{\epsilon}_p > \dot{\epsilon}_p^{c/t} \end{cases}, \quad (5)$$

where $\dot{\epsilon}_p^{c/t}$ is 30 s⁻¹, $\gamma_{c/t}$ is computed from a continuity requirement, and the default values are $\beta_c = 0.032$, $\beta_t = 0.036$. In this study, we tried to calibrate β_c and β_t equally for the simplicity of calibration, and DIF values according to various β_c and β_t are represented in Fig. 9. As the β_c and β_t value increases, the DIF value increases. The values were calibrated to appropriate values through computational analysis of the smoothbore test.

Finite-element analysis of the smoothbore gun test for various β_c and β_t values was carried out using the dynamic structural analysis tool LS-DYNA v.971 R12 with an explicit solver. Before performing finite-element analysis, finite-element models of a target and test projectile were generated, and half modeling using the symmetric boundary conditions is adopted for the time efficiency of analysis. To improve the accuracy of the analysis, the concrete target is modeled as a mixture of FEM and SPH. The part where a large amount of

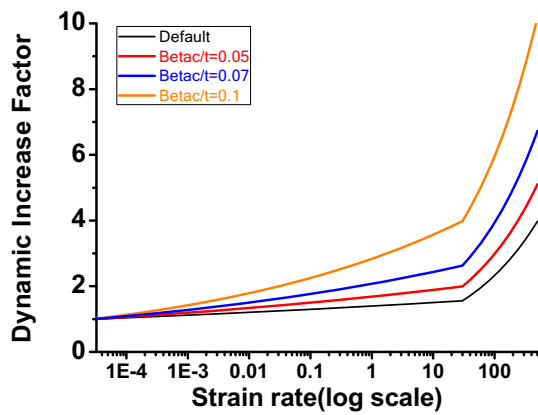


Fig. 9 Dynamic increase factor with various β_c/β_t values

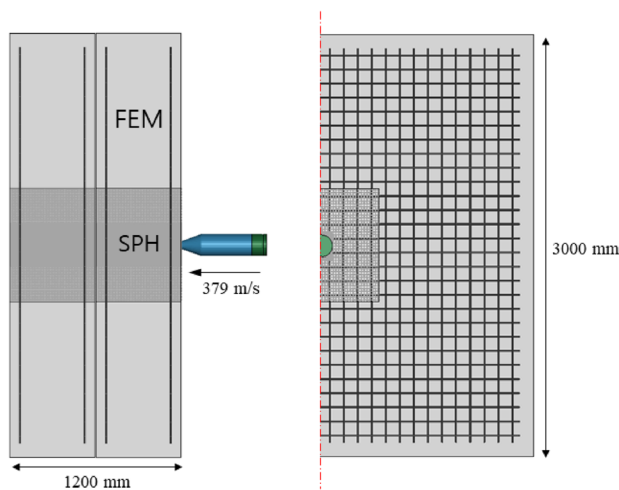


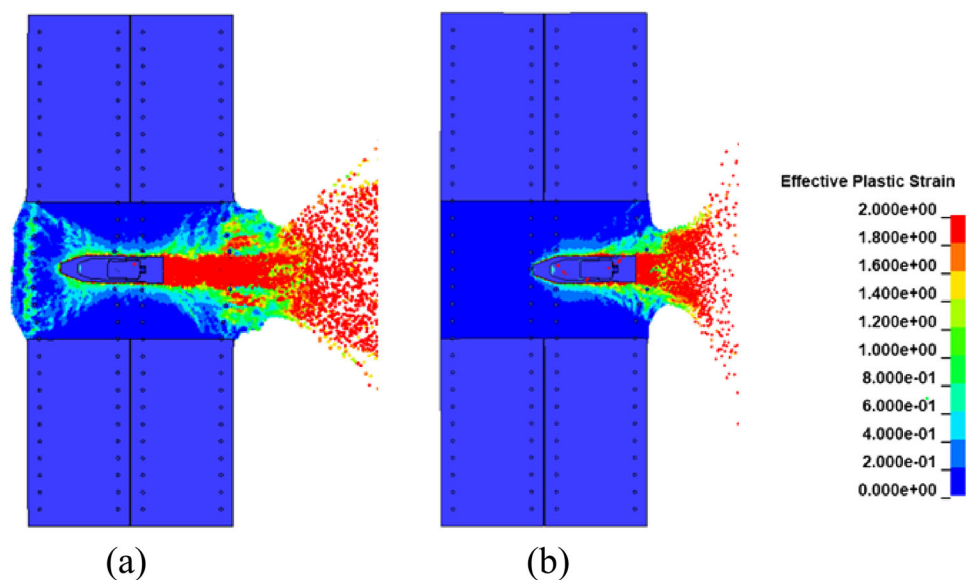
Fig. 10 Numerical modeling of smoothbore gun test

deformation was expected from the impact with a test projectile was modeled as the SPH domain, and the surrounding region was modeled with the FEM domain using hexahedral elements. In addition, the rebar in the concrete was modeled with hexahedral elements, and a mixture of constrained and contact conditions was applied. Since the SPH technique is sensitive to internode spacing, the SPH node-to-node spacing of the concrete target was fixed to 7 mm to secure converged results with respect to the mesh size. Finite-element modeling was carried out using a sufficiently large number of nodes and elements, and the results are shown in Fig. 10.

As a boundary condition in the finite-element analysis for the smoothbore gun test, contact conditions between the test projectile and the target were set, as shown in Fig. 10. Furthermore, contact conditions were set between the targets, simulating the transmission of the shock wave. The rear part of the target was constrained in the direction of the test projectile and the penetration speed of the test projectile was set to 379 m/s. The material properties of the test projectile were adopted from the constitutive equation of AISI 4340 steel obtained in Sect. 2, and the fracture condition was not entered with reference to the test results. The concrete target used the RHT model, and a default value corresponding to an unconfined compressive strength of 5000 psi, except for β_c/β_t was set.

The results of finite-element analysis for various β_c and β_t values are shown in Figs. 11 and 12, respectively. Figure 11 shows effective plastic strain after target penetration. The distribution of plastic strain in the target and the depth of penetration of the test projectile were different with respect to the β_c and β_t values. It can be inferred that the DIF value varies according to β_c and β_t , and the target resistance stress differs accordingly. Figure 12 shows the penetration depth

Fig. 11 Simulation results of smoothbore gun test with various β_c and β_t values. **a** Default and **b** 0.08



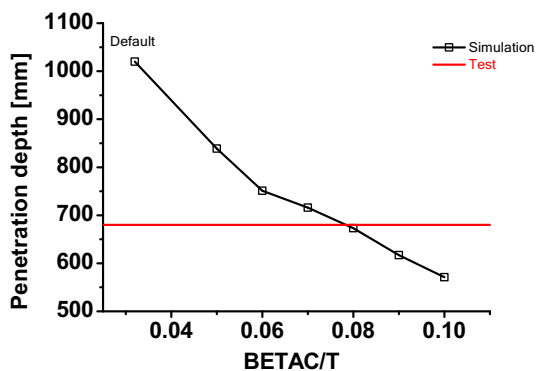


Fig. 12 Penetration depth of smoothbore gun test with various β_c and β_t values

for various $\beta_{c/t}$. The penetration depth decreased as the $\beta_{c/t}$ value increased, and the sensitivity according to $\beta_{c/t}$ was significant. The test result was 680 mm as mentioned before, and the $\beta_{c/t}$ value that best simulates this was 0.08. The strain rate of an SPH node is in the order of thousands s^{-1} , and maximum value is about $10,000 s^{-1}$. Therefore, 0.08 was selected as the β_c and β_t value of the RHT model to well represent the behavior of concrete at the strain rate up to thousands s^{-1} .

4 Warhead Survivability Assessment

To assess the structural survivability of the projectile through correlated simulation, the dynamic constitutive equation and dynamic fracture properties of the projectile material were obtained. Additionally, the coefficients of material property model for the target material were calibrated through the smoothbore gun test. Using this, correlated simulation was carried out on the concrete oblique impact sled test with the projectile, as penetration test in [30]. By comparative analysis with the test results, the usefulness of the proposed

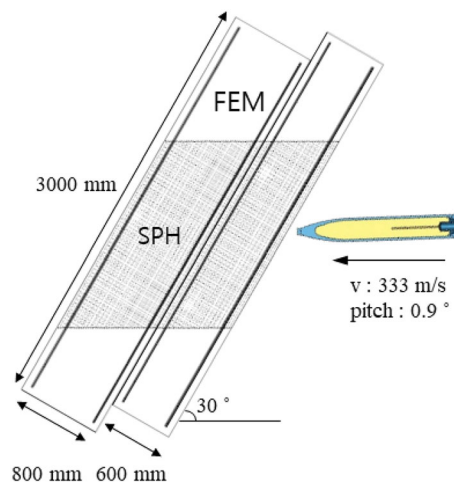


Fig. 14 Numerical modeling of sled penetration test

computational analysis technique was confirmed. As shown in Fig. 13, the test in [30] confirmed that a projectile with a mass of 232 kg hit a concrete target with a compressive strength of 5000 psi at a speed of 333 m/s and an inclination angle of 30° . The projectile failed to penetrate the target and was destroyed.

For the computational analysis of the penetration test in [30], LS-DYNA v.971 R12 with an explicit solver was utilized. Computational modeling was carried out as shown in Fig. 14 as half model. To improve the accuracy of the analysis, the concrete target was modeled as a mixture of FEM and SPH, and the rebar in the concrete was modeled with hexahedral elements. The spacing between SPH nodes was set to 7 mm, and 1.6 million SPH nodes and 78,000 hexahedral elements were used. The boundary between SPH nodes and FEM elements was determined as the area where no significant plastic deformation occurred on concrete target. The projectile was modeled using 38,000 nodes and 32,000 hexahedral elements. The size of element in the projectile wall

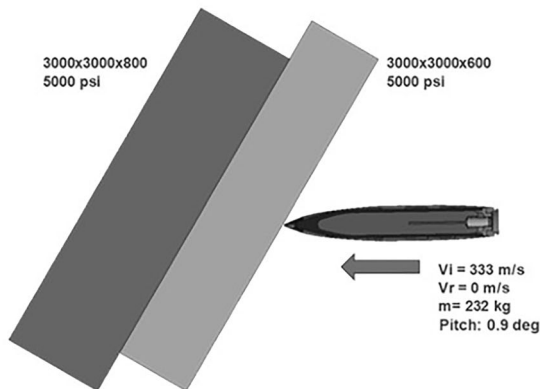


Fig. 13 Penetration test in [30]

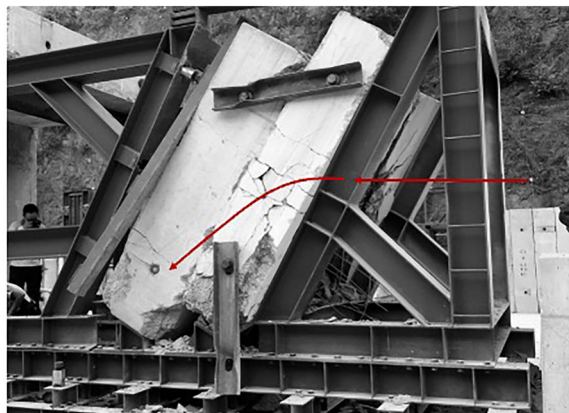
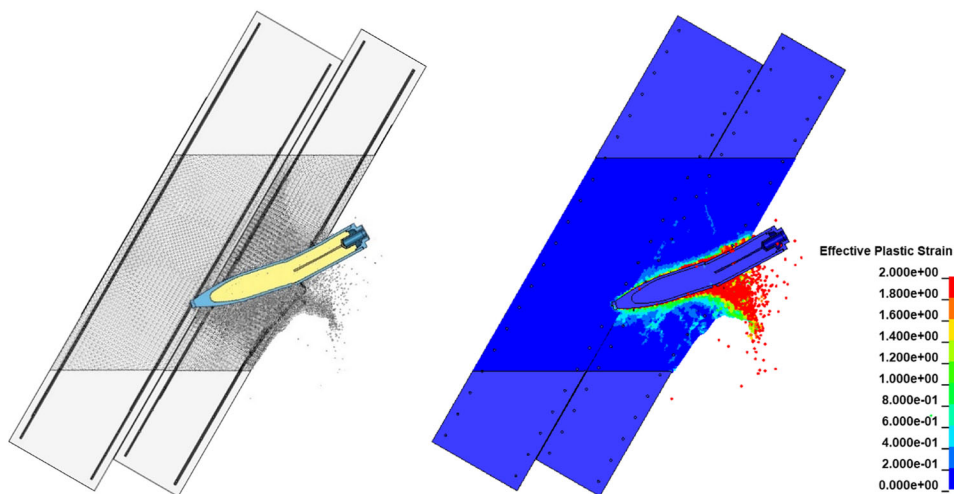


Fig. 15 Simulation results of sled penetration test



where fracture was predicted was selected as 3 mm from the mesh size regularization result in Sect. 2.3.

As boundary conditions for the analysis, contact conditions were applied between the projectile and target and among the targets. The TIE conditions were applied on target elements and rebar elements. The rear part of the target was constrained in the direction of the projectile and the penetration speed of the projectile was set to 333 m/s. Based on the computational analysis application technique in Sect. 2.3, the constitutive equation and fracture model of the AISI 4340 steel obtained in Sect. 2 was entered to the analysis. The concrete target material model was the RHT model, with a $\beta_{c/t}$ value of 0.08. Finite-element analysis was carried out using 16 CPU cores on a workstation equipped with an Intel Xeon CPU (24 cores, 3.0 GHz) and 192 GB memory. The computation time was approximately 72 h.

The results of finite-element analysis for warhead structural survivability assessment are shown in Figs. 15 and 16. Figure 15 shows the results of the analysis, showing the depth and posture of the penetration warhead at 5 ms after target penetration, and the degree of deformation including the projectile fracture. Results shows that the projectile failed to penetrate the second layer after penetrating the first slab. It was tilted down at about 15°, and the deformation concentration occurred in the center wall of the projectile which caused a fracture. According to the results of the Penetration test [30], the penetrating warhead penetrated the first concrete target slab but failed to penetrate the second slab. The projectile fractured at the center wall of the projectile. Therefore, it can be confirmed that the finite-element analysis results have a good agreement with the test results. In addition, the strain rate of an SPH node in this analysis was in the order of thousands s^{-1} , and maximum value was about 9000 s^{-1} which confirmed the used $\beta_{c/t}$ value was appropriate.

Figure 16 shows the distribution of the damage values of the projectile in relation to warhead survivability over time after the target impact. In Fig. 16b, bending caused by asymmetric target resistance occurred as the projectile hit the target obliquely, thereby creating damage to the center of the projectile. Figure 16c shows that the projectile has a reverse bend and an increase in damage values as penetration continues. Figure 16d shows that the increasing damage value reaches 1, and fracture occurs at the center wall of the projectile.

To identify the mechanism of projectile fracture during penetration, the stress state of the fractured element of the projectile is shown in Fig. 17. It illustrates stress triaxiality and Lode angle parameters over time. The stress state changed due to projectile deformation as the penetration progressed. At the beginning of penetration, tremors of the stress state due to shock were observed. Then, up to about 2.2 ms, the stress triaxiality was around $-1/3$ and the Lode angle parameter was around -1 which shows compression state due to bending. As the penetration progressed, the stress triaxiality was around $1/3$ and the Lode angle parameter was around 1 resulting in a tension state due to reverse bending on the projectile. Then, the damage value increased and fracture occurred. Therefore, by assessing the projectile structural survivability through this finite-element analysis, warhead survivability in the penetration test can be predicted. In the event of a fracture, the direction for improving the warhead design can be confirmed through this loading path analysis.

5 Conclusion

In this study, structural survivability assessment was carried out through correlated simulation on the penetration of projectile in a concrete target of two slabs. The analysis was verified by comparing it with test results. For correlated

Fig. 16 Distribution of damage on the projectile body after impact time of: **a** 0; **b** 1.5; **c** 3.0; and **d** 3.5 ms

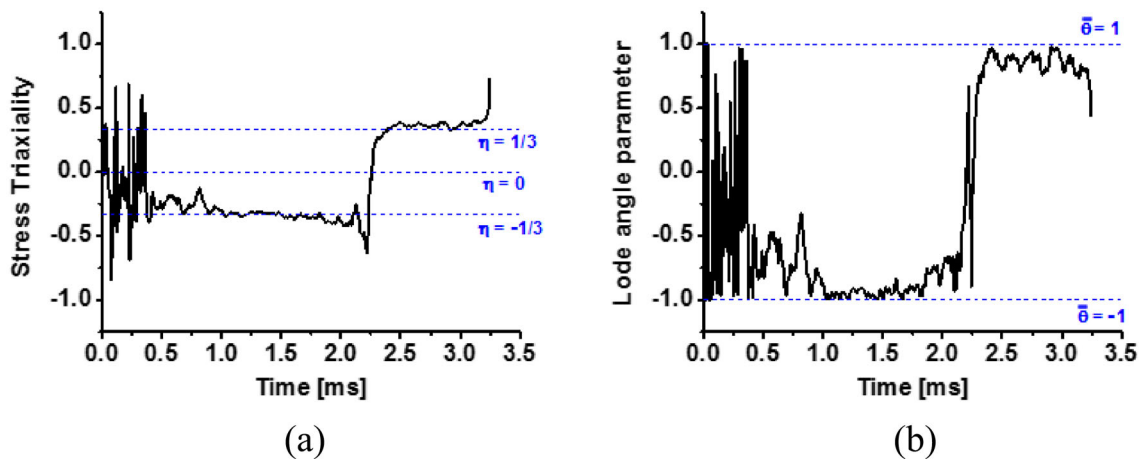
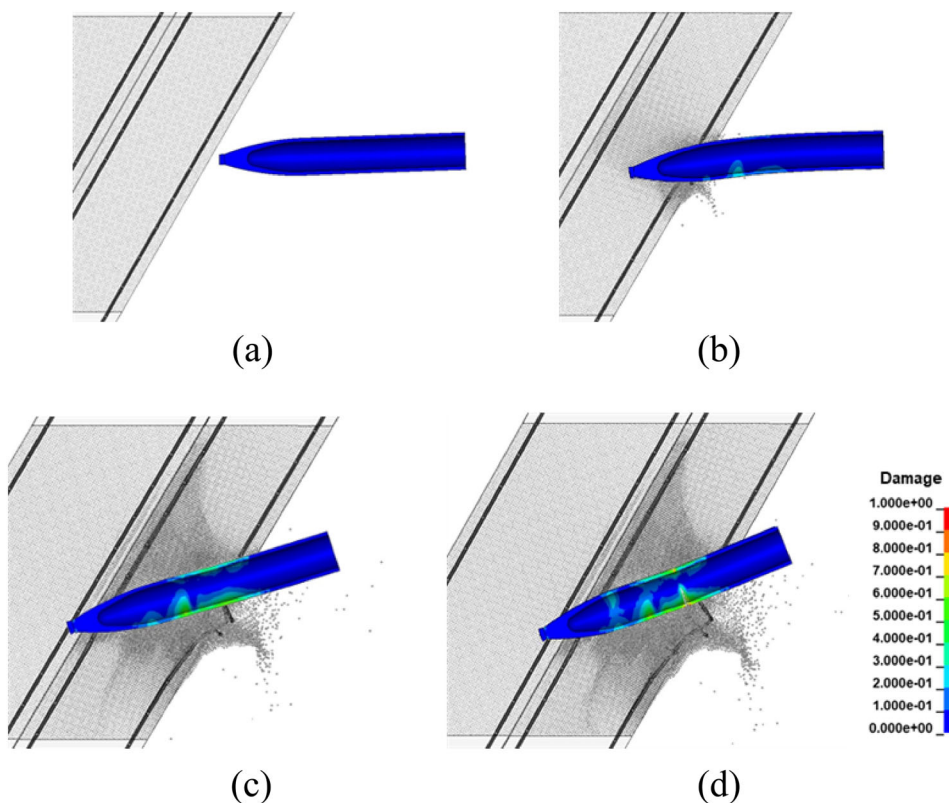


Fig. 17 Stress states of the deleted element during penetration: **a** stress triaxiality and **b** Lode angle parameter

simulation, material property modeling that can express the behavior of the projectile material under extreme load conditions was carried out, and a fracture model with respect to strain rate was constructed. To obtain accurate target properties, penetration tests were conducted using 155 mm smoothbore guns to obtain the coefficients of the concrete material model that can best simulate the test results. Then, a correlated simulation was carried out on the Penetration test in [30] in which the projectile was damaged. Similar to the

test results, it was possible to verify the validity of the proposed computational analysis technique by confirming that the fracture during penetration of the penetration warhead was well predicted.

By extending this study, it will be possible to assess structural survivability at various impact velocities and penetration variables in the future. It will require the implementation of constitutive equations of materials and fracture models that can take into account various variables. Moreover, accurate calibration of target properties and the improvement of

computational efficiency is necessary. The proposed techniques for warhead structural survivability assessment will be applied to the warhead design process to reduce the number of penetration tests conducted while optimizing its performance.

Acknowledgements This work was supported by the Agency for Defense Development by Korean Government (912805201)

Declarations

Conflict of Interest On behalf of all authors, the corresponding author states that there is no conflict of interest.

References

- Young CW (1997) Penetration equations. SAND97-2426. Sandia National Laboratories, USA
- Forrestal MJ, Altman BS, Cargile JD, Hanchak SJ (1994) An empirical equation for penetration depth of ogive nose projectiles into concrete targets. *Int J Impact Eng* 15(4):395–405. [https://doi.org/10.1016/0734-743X\(94\)80024-4](https://doi.org/10.1016/0734-743X(94)80024-4)
- Forrestal MJ, Frew DJ, Hickerson JP, Rohwer TA (2003) Penetration of concrete targets with deceleration-time measurements. *Int J Impact Eng* 28(5):479–497. [https://doi.org/10.1016/S0734-743X\(02\)00108-2](https://doi.org/10.1016/S0734-743X(02)00108-2)
- Choi MK, Han J, Park S, An WJ (2018) Efficient method to evaluate critical ricochet angle of projectile penetrating into a concrete target. *Math Probl Eng*. <https://doi.org/10.1155/2018/3696473>
- Liu Y, Ma A, Huang F (2009) Numerical simulations of oblique angle penetration by deformable projectiles into concrete targets. *Int J Impact Eng* 36(3):438–446. <https://doi.org/10.1016/j.ijimpeng.2008.03.006>
- Liu Y, Huang F, Ma A (2011) Numerical simulations of oblique penetration into reinforced concrete targets. *Comput Math Appl* 61(8):2168–2171. <https://doi.org/10.1016/j.camwa.2010.09.006>
- Zukas JA (1990) High velocity impact dynamics. John Wiley & Sons Inc, New Jersey
- Popelar CH, Walker JD, Anderson Jr CE, Johnson GR, Beissel SR (1999) Penetrator case fracture predictive technology. AFRL-MN-EG-TR-1999-7054. Air Force Research Laboratory
- Yoo YH, Kim JB, Lee CW (2019) Effects of the projectile geometries on normal and oblique penetration using the finite cavity pressure method. *Appl Sci* 9(18):3939. <https://doi.org/10.3390/ap9183939>
- Lim SJ (2017) A ductile fracture criterion of sheet metals at a wide range of strain rates. PhD dissertation. KAIST
- Johnson GR, Cook WH (1983). A constitutive model and data for metals subjected to large strains, high strain rates and high temperatures. In: Proceedings of the seventh international symposium on ballistics, The Netherlands
- Huh H, Ahn K, Lim JH, Kim HW, Park LJ (2014) Evaluation of dynamic hardening models for BCC, FCC, and HCP metals at a wide range of strain rates. *J Mater Process Technol* 214(7):1326–1340. <https://doi.org/10.1016/j.jmatprotec.2014.02.004>
- Shin H, Ju Y, Choi MK, Ha DH (2022) Flow stress description characteristics of some constitutive models at wide strain rates and temperatures. *Technologies* 10(2):52. <https://doi.org/10.3390/tech10020052>
- Lemaitre J, Desmorat R (2005) Engineering damage mechanics. Springer-Verlag, New York
- Gurson AL (1977) Continuum theory of ductile rupture by void nucleation and growth: Part I. Yield criteria and flow rules for porous ductile media. *J Eng Mater Technol* 99(1):2–15. <https://doi.org/10.1115/1.3443401>
- Tvergaard V, Needleman A (1984) Analysis of the cup-cone fracture in a round tensile bar. *Acta Metall Mater* 32(1):157–169. [https://doi.org/10.1016/0001-6160\(84\)90213-X](https://doi.org/10.1016/0001-6160(84)90213-X)
- Neukamm F, Feucht M, Haufe A, Roll K (2008) On closing the constitutive gap between forming and crash simulation. In: 10th International LS-DYNA users conference, vol 12, pp 21–32
- Wierzbicki T, Bao Y, Lee YW, Bai Y (2005) Calibration and evaluation of seven fracture models. *Int J Mech Sci* 47(4–5):719–743. <https://doi.org/10.1016/j.ijmecsci.2005.03.003>
- Bai Y, Wierzbicki T (2010) Application of extended Mohr–Coulomb criterion to ductile fracture. *Int J Fract* 161(1):1–20. <https://doi.org/10.1007/s10704-009-9422-8>
- Lou Y, Huh H, Lim S, Pack K (2012) New ductile fracture criterion for prediction of fracture forming limit diagrams of sheet metals. *Int J Solids Struct* 49(25):3605–3615. <https://doi.org/10.1016/j.jiistr.2012.02.016>
- Roth CC, Mohr D (2014) Effect of strain rate on ductile fracture initiation in advanced high strength steel sheet: experiment and modeling. *Int J Plast* 56:19–44. <https://doi.org/10.1016/j.ijplas.2014.01.003>
- Teng X, Wierzbicki T, Hiermaier S, Rohr I (2005) Numerical prediction of fracture in the Taylor test. *Int J Solids Struct* 42(9–10):2929–2948. <https://doi.org/10.1016/j.ijsolstr.2004.09.039>
- Zhang W, Xiao X, Wei G, Guo Z (2012) Evaluation of five fracture models in Taylor impact fracture. *AIP Conf Proc* 2012(1426):1125–1128. <https://doi.org/10.1063/1.3686477>
- Xiao X, Mu Z, Pan H, Lou Y (2018) Effect of the Lode parameter in predicting shear cracking of 2024–T351 aluminum alloy Taylor rods. *Int J Impact Eng* 120:185–201. <https://doi.org/10.1016/j.ijimpeng.2018.06.008>
- Riedel W, Kawai N, Kondo K (2009) Numerical assessment for impact strength measurements in concrete materials. *Int J Impact Eng* 36(2):283–293. <https://doi.org/10.1016/j.ijimpeng.2007.12.012>
- Malvar LJ, Crawford JE, Wesevich JW, Simons D (1997) A plasticity concrete material model for DYNA3D. *Int J Impact Eng* 19(9–10):847–873. [https://doi.org/10.1016/S0734-743X\(97\)00023-7](https://doi.org/10.1016/S0734-743X(97)00023-7)
- Murray YD (2007) Users manual for LS-DYNA concrete material model 159. FHWA-HRT-05-062. Federal Highway Administration
- Hansson H, Skoglund P (2002) Simulation of concrete penetration in 2D and 3D with the RHT material model. FOI-R-0720-SE. Swedish Defense Research Agency
- Shin W, Park H, Han J (2022) Improvement of the dynamic failure behavior of concrete subjected to projectile impact using user-defined material model. *Constr Build Mater* 332:127343. <https://doi.org/10.1016/j.conbuildmat.2022.127343>
- Kim SB, Kim HW, Yoo YH (2015) Penetration analysis of projectile with inclined concrete target. *EPJ Web Conf* 94:04052. <https://doi.org/10.1051/epjconf/20159404052>
- Lim J (2005) Study on dynamic tensile tests of auto-body steel sheet at the intermediate strain rate for material constitutive equations. PhD dissertation. KAIST
- Huh H, Kang WJ, Han SS (2002) A tension split Hopkinson bar for investigating the dynamic behavior of sheet metals. *Exp Mech* 42(1):8–17. <https://doi.org/10.1007/BF02411046>
- Pack K (2012) Study on the fracture strain of DP780 sheets considering the strain rate and loading path. Masters thesis. KAIST
- Lim SJ, Huh H (2017) Fracture loci of DP980 steel sheet for auto-body at intermediate strain rates. *Int J Automot Technol* 18(4):719–727. <https://doi.org/10.1007/s12239-017-0071-z>

35. Lou Y, Huh H (2013) Evaluation of ductile fracture criteria in a general three-dimensional stress state considering the stress triaxiality and the Lode parameter. *Acta Mech Solida Sin* 26(6):642–658. [https://doi.org/10.1016/S0894-9166\(14\)60008-2](https://doi.org/10.1016/S0894-9166(14)60008-2)
36. Kõrgesaar M (2015). Modeling ductile fracture in ship structures with shell elements. Doctoral dissertation. Aalto University
37. Kõrgesaar M, Remes H, Romanoff J (2014) Size dependent response of large shell elements under in-plane loading. *Int J Solids Struct* 51:3752–3761
38. Li Y, Karr DG (2009) Prediction of ductile fracture in tension by bifurcation, localization, and imperfection analyses. *Int J Plast* 25(6):1128–1153. <https://doi.org/10.1016/j.ijplas.2008.07.001>
39. Cho H, Choi MK, Park S, Kim M, Han J, Sohn D (2022) Determination of critical ricochet conditions for oblique impact of ogive-nosed projectiles on concrete targets using semi-empirical model. *Int J Impact Eng* 165:104214. <https://doi.org/10.1016/j.ijimpeng.2022.104214>
40. Beton C-E-I (1993) CEB-FIP model code 1990: design code. Thomas Telford Publishing, London
41. Malvar LJ, Ross CA (1998) Review of strain rate effects for concrete in tension. *ACI Mater J* 95(7355):7
42. Borrvall T, Riedel W (2011) THE RHT concrete model in LS-DYNA. In: 8th European LS-DYNA users conference

Publisher's Note Springer Nature remains neutral with regard to jurisdictional claims in published maps and institutional affiliations.

Springer Nature or its licensor (e.g. a society or other partner) holds exclusive rights to this article under a publishing agreement with the author(s) or other rightsholder(s); author self-archiving of the accepted manuscript version of this article is solely governed by the terms of such publishing agreement and applicable law.